Applied Catalysis B: Environmental 197 (2016) 244–253

Contents lists available at ScienceDirect

Applied Catalysis B: Environmental

journal homepage: www.elsevier.com/locate/apcatb

The role of ceria in LSM-GDC composite cathode for electrochemical reduction of nitric oxide

Wenyi Tan[a,b,*], Fei Chen[a], Lei Gong[a], Huangang Shi[a], Qin Zhong[b]

[a] Department of Environment Engineering, Nanjing Institute of Technology, Nanjing, 211167 Jiangsu, China
[b] School of Chemical Engineering, Nanjing University of Science & Technology, Nanjing, 210094 Jiangsu, China

ARTICLE INFO

Article history:
Received 14 October 2015
Received in revised form 9 February 2016
Accepted 11 February 2016
Available online 22 February 2016

Keywords:
Nitric oxide
Electrochemical reduction
Ceria
Solid state cell reactor (SSCR)

ABSTRACT

Electrochemical reduction of nitric oxide (NO) in a solid state cell reactor (SSCR) is conducted at intermediate-temperature (500–550 °C) using three $(La_{0.85}Sr_{0.15})_{0.9}MnO_3$ (LSM)-$Ce_{0.8}Gd_{0.2}O_2$ (GDC) composite cathodes (LSM:GDC = 3:1, 2:2 and 1:3 wt.%, denoted respectively as LSM-GDC31, LSM-GDC22, and LSM-GDC13). GDC-free LSM cathode is compared as blank sample. The NO conversion and current generation are evaluated. In the absence of oxygen, NO apparent conversion at the closed circuit state at 550 °C is almost 60%, and the corresponding current density at 0.3 V is 17 mA cm^{-2} with LSM-GDC22. NO apparent conversion and current produced are greatly enhanced up to 80% and 66.7 mA cm^{-2} in 2000 ppm NO-10% O_2 at 500 °C due to the electrochemical promotion of catalysis (EPOC). The combined electrochemical impedance spectra, in-situ diffuse reflectance infrared fourier transform spectra, scanning electron microscope and Raman spectra are applied and prove that the oxygen-storage properties of ceria improves the selectivity towards NO electrochemical reduction in oxygen-rich atmosphere. In addition, the introduction of GDC enhances the electrode activities due to the increased three phase boundary (TPB) for oxygen reduction reaction.

1. Introduction

Diesel engines are gaining more attention than gasoline engines because of its highly efficiency, durability and lower CO_2 emission. However, a great amount of NOx from the exhaust, detrimental to atmospheric environment and human health, obstructs wide applications of diesel engines. In order to meet the tougher emission standard, a lean-burn engine with excess oxygen supply is needed, which is equipped with a complicated auxiliary system, including urea-selective catalytic reduction (SCR), exhaust gas recirculation (EGR) and so on [1,2].

In 1990s, Hibino and Kobayashi proposed the reduction of NOx in electrochemical cells [3,4]. Later, Kammer's group and Huang et al. introduced solid state cell reactor (SSCR) for the purpose of exhaust purification in a recent decades [5–7]. Due to high contents of oxygen and 200–1000 ppm levels of NOx present in the exhaust from diesel engines, electrode activity and selectivity towards NO reduction in operating temperatures have been investigated intensively. For example, cone-shaped electrodes composed of simple oxides (e.g. NiO and CuO), spinels (e.g. $CuCr_2O_4$), perovskite oxides such as $La_{1-x}Sr_xMnO_3$, $La_{0.85}Sr_{0.15}CoO_3$ and $La_{0.6}Sr_{0.4}Mn_xFe_{1-x}O_3$ etc have been employed as cathodes in the SSCR [5]. It has been found that these electrodes showed acceptable performances only above 500 °C. Huang adopted solid oxide fuel cell (SOFC)-DeNOx technology to remove NOx by feeding reductant (e.g. H_2) into anode chamber [7,8]. As a result, the NOx conversion increased with the increase in NOx concentration at 700–800 °C under the open circuit voltage (OCV) conditions. Furthermore nearly 8 mW cm^{-2} was achieved at 750 °C when NOx acted as the only oxidant instead of O_2 [9].

Previously, yttria-stabilized zirconia (YSZ) electrolyte was the preference in SSCR for SOFC-DeNOx technology. However, a relative high temperature (above 800 °C) is required for YSZ to yield high oxygen ion conductivity, while the temperature range is far beyond that of exhausts gas. Therefore, issues including thermal stability of materials and an additional heating system are bound to be considered [10,11]. Ceria based materials possess a relatively high conductivity at intermediate temperatures (600–700 °C), which also exhibits physicochemical activities for exhaust gas [12,13]. When a composite cathode containing ceria are employed to reduce NO in an electrochemical way, it brings new insights into the electrochemical reduction for NO in exhaust gas. In this paper, a SSCR with the configuration of $(La_{0.75}Sr_{0.25})_{0.95}MnO_3$

* Corresponding author at: Department of Environment Engineering, Nanjing Institute of Technology, Nanjing, 211167 Jiangsu, China.
E-mail addresses: twy1102@gmail.com, twy9@sina.com (W. Tan).

http://dx.doi.org/10.1016/j.apcatb.2016.02.029
0926-3373/

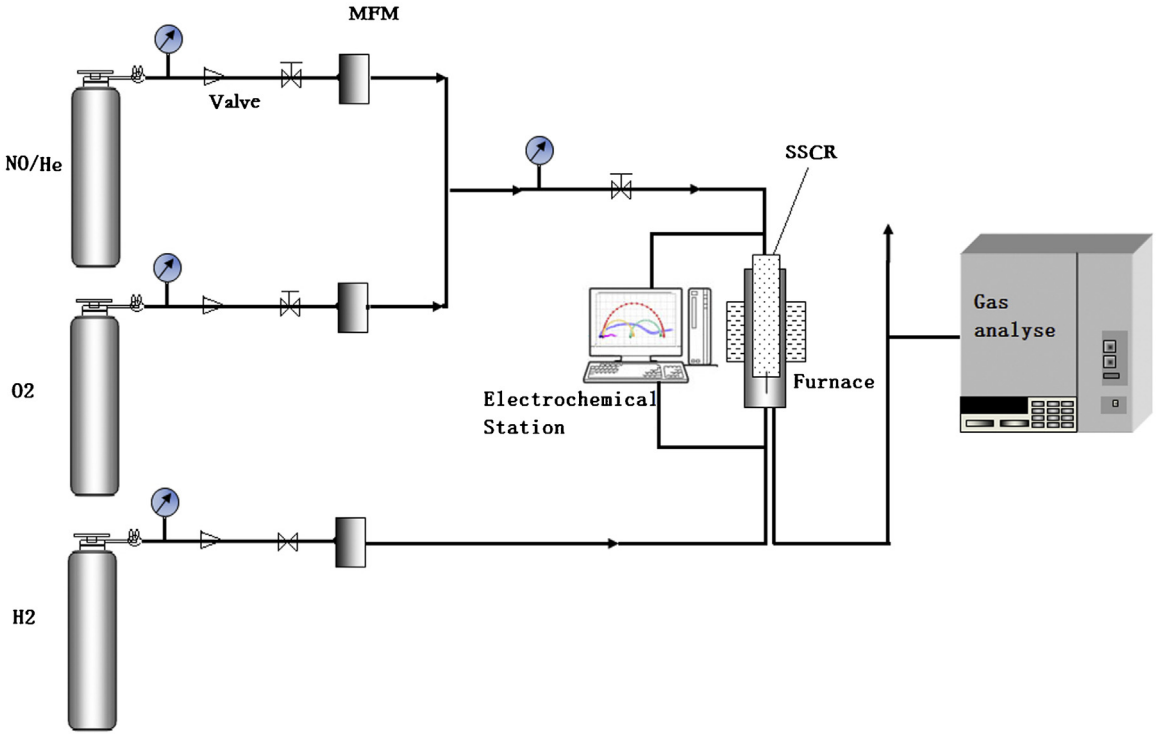

Fig. 1. A SSCR diagram for NO electrochemical reduction.

(LSM)-GDC/GDC/Ni-GDC was fabricated. Various amounts of Gd-doped ceria (GDC) were introduced into the LSM cathodes in the SSCR for the NO abatement in the presence and absence of O_2, aiming to explore the potential synergistic effect of LSM and GDC in the electrochemical reduction of NO.

2. Experiments

2.1. Materials preparation

The LSM powders in this study were purchased from NIMTE (China). GDC powders were synthesized by glycine nitric process (GNP) method as described elsewhere [14]. In brief, a stoichiometric amount of Gd_2O_3 (Sino-pharm, China) was dissolved in nitric acid first, and then $Ce(NO_3)_3{\cdot}6H_2O$ and an excess of citric acid as fuel were added. The solution was heated on a hot plate until the combustion happened, then the obtained precursor powders were calcined at 1000 °C in air for 4 h.

LSM and GDC powders were mixed to act as composite cathodes with various weight ratios of 3:1, 2:2, 1:3 (denoted as LSM-GDC31, LSM-GDC22 and LSM-GDC13, respectively). The mixed powders were ball-milled for 10 h. Then all powders were calcined at 1200 °C for 4 h. A ceria-free powder was also proceeded to act as blank cathode. After calcination of $Ni(NO_3)_2{\cdot}H_2O$ at 650 °C for 3 h, NiO were obtained and then mixed with GDC powders (70:30 wt.%) to prepare anode powders.

2.2. SSCR fabrication

An electrolyte-supported solid state cell was fabricated. The module was filled with the weighed GDC powders, which were then isostatically pressed into a disc with a diameter of 15 mm and a thickness of 0.2 mm. The disc-like electrolyte was calcined at 1350 °C for 6 h. To prepare cathode and anode slurry, LSM-GDC and NiO-GDC powders were mixed with turpentine oil, respectively. The obtained slurries were painted onto the corresponding sides of the dense electrolyte disc. Finally, the cell with a thickness of ~0.25 mm was calcined at 1200 °C for 4 h. The obtained solid state cell was sealed by silver paste onto a quartz tube.

2.3. Catalyst characterizations and measurements

Crystal structures of the synthesized powders were determined by X-ray diffraction (XRD, Bruker D8 ADVANCE) using CuKα radiation ($\lambda = 1.54060$ Å, $2\theta = 5 - 80°$) with the step of 0.02° at room temperature.

Raman spectra of four cathodes were collected using Renishaw inVia equipped with an Ar^+ laser source of wavelength 532 nm. A field emission scanning electron microscope (FE-SEM, HITACHI-S4800) was used to characterize the microstructure.

In situ diffuse reflectance infrared fourier transform spectra (DRIFTS) was conducted using a Nicolet iZ10 FTIR spectrometers with NaCl windows which was connected to a gas system to allow measurements under the controlled atmosphere at 1 atm and temperatures up to 400 °C. Prior to the tests, the catalysts in the DRIFTS cell were pretreated at 300 °C in He for 2 h and then cooled to the 250 °C. After exposure to He stream for recording the background spectrum, the atmosphere was switched to 2000 ppm NO for measurements.

Electrochemical reduction of NO was performed in the fabricated SSCR at 500 and 550 °C. Prior to electrochemical tests, pure H_2 was fed into anode side at 500 °C and kept for 1 h in order to reduce NiO to Ni completely, while air was pumped into the cathode. Until the open circuit voltage (OCV) elevated up to a stable value of 1.01 V, which is near the theoretical value of H_2-air SOFC, air flow was switched to 1000–3000 ppm NO balanced by He. A high OCV achieved suggested that the GDC electrolyte was dense and no obvious leakage took place. The flow rates of all streams were controlled by mass flow controllers at 150 mL min^{-1}. For the purpose of comparison, the currents were detected at a unified voltage (0.3 V) by milliammeter (D26, Nanjing). The NO concentrations of inlet and outlet were monitored by a Flue Gas Analyzer (Germany

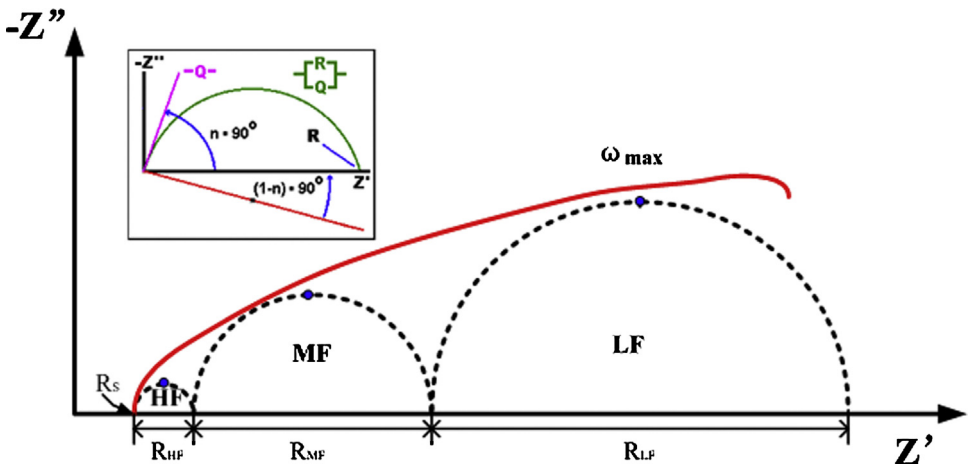

Fig. 2. Illustration for AC impedance spectra analysis.

ECOM-JZKN), either under a fixed-voltage of 0.3 V or under OCV conditions. The NO conversion (X_{NO}) can be calculated with the Eq. (1).

$$X_{NO}(\%) = \frac{[NO]_{inlet} - [NO]_{outlet}}{[NO]_{inlet}} \times 100\% \quad (1)$$

The schematic diagram is shown in Fig. 1.

2.4. Electrochemical tests and electrochemical impedances spectra (EIS)

In order to evaluate electrochemical activity of cathodes exposure to NO or NO-O_2, a symmetrical cell fabricated with identical electrodes coated on GDC film was tested by an electrochemical station (VersaSTAT 3, Ametek, USA) at open circuit mode in the frequency range of 100 kHz–0.1 Hz. EIS were recorded at 10 points per decade with an AC perturbation of 5 mV.

Electrochemical reaction processes for the NO electrochemical reduction can be identified by EIS. As illustrated in Fig. 2., EIS expressed in Nyquist plot usually include several overlapping arcs. The impedance spectra was fitted with a certain equivalent circuit with the combination of ideal (resistor *R*, capacitor *C*, inductor *L*, etc.) and non-ideal (constant phase element or CPE, Warburg, etc.) electrical elements in series and/or in parallel [15–17]. An appropriate equivalent circuit should show low chi-squared parameters and have physical/chemical meanings. These arcs correspond to different electrode processes. Typically, an equivalent circuit $LR_S(RQ)_H(RQ)_M(RQ)_L$ can be used to fit the impedance spectra and thus the related physical/chemical processes in different frequencies can be distinguished. The inductance *L* is primarily ascribed to the leads and current collectors. The serial resistance R_S, corresponding to the onset point in high frequency at the real axis, is ascribed to the total resistances including electrodes and electrolyte. The three sub-circuits *(RQ)* composed of the resistance *R* and constant phase element (CPE, symbolized by *Q*) are assigned to the elements in high, medium and low frequencies. *R* values in different frequencies are obtained according to the corresponding intercepts, and the total polarization resistance (R_p) is the sum of individual polarization resistances. The constant phase element (*Q*) value can be expressed as:

$$Z = \frac{1}{Y_0(j\omega)^n} \quad (2)$$

where Y_0 is |Z|, ω is the angle frequency and n is the frequency exponent (n = 0–1, describes the heterogeneous or porous character).

When n = 1, this is the same equation as that for the impedance of a capacitor,

$$Z = \frac{1}{j\omega Y_0} = \frac{1}{j\omega C_\omega} \quad (3)$$

where $Y_0 = C_\omega$. When n is close to 1.0, the CPE resembles a capacitor, but the phase angle is not 90°. It is constant and somewhat less than 90° at all frequencies. In some cases, the ‘true’ capacitance can be calculated from Y_0 and n:

$$C_\omega = (R^{1-n}Y_0)^{\frac{1}{n}} \quad (4)$$

The summit frequency of arc can be calculated as follows.

$$f_{max} = \left(\frac{1}{2\pi}\right)(RY_0)^{\frac{1}{n}} \quad (5)$$

3. Hypothesis for NO electro-reduction

The possible pathways for NO electrochemical reduction in the absence and presence of O_2 are summarized below, in order to understand the following discussions better.

3.1. In the absence of O_2

There are two possible reactions for electrochemical reduction of NO:

$$2NO + 2H_2 = N_2 + 2H_2O \quad (6)$$

$$O_2 + 2H_2 = 2H_2O \quad (7)$$

The reaction (6) can be divided into two half-cell reactions (8) and (9):

$$2NO + 2e = \frac{1}{2}N_2 + O^{2-} \quad (8)$$

$$H_2 + O^{2-} = 2H_2O + 2e \quad (9)$$

According to the Nernst equation, the theoretical OCVs of Reactions (6) and (7) at 25 °C are 1.68 V and 1.20 V, respectively. Therefore we can judge the reactions from OCV since OCV in the Reaction (7) is proportional to the oxygen partial pressure (pO_2). Oxygen derived from NO decomposition is trapped by Ce(III) with oxygen vacancies when GDC was introduced into the LSM based cathodes. Thus, according to the Reaction (7), the low pO_2 results in low OCV values.

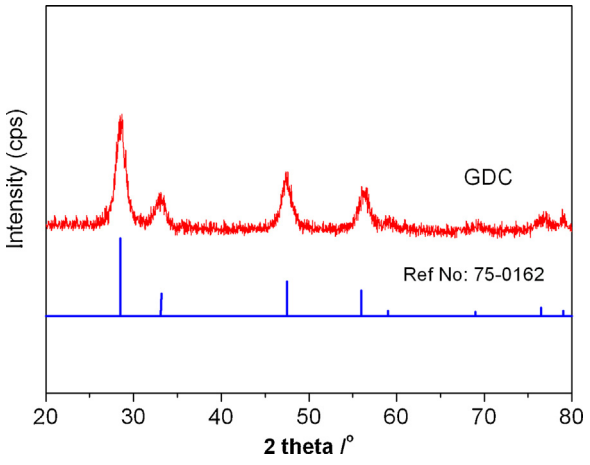

Fig. 3. XRD patterns of the synthesized GDC powders.

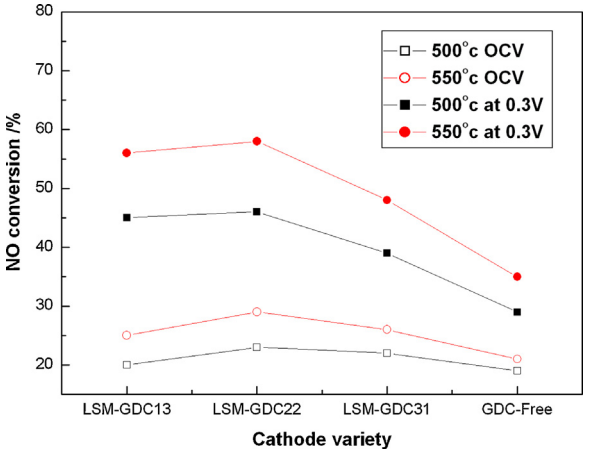

Fig. 4. NO conversion as the function of GDC content under OCV conditions and at the voltage of 0.3 V.

3.2. In the presence of O2

The increasing content of ceria in the composite cathodes contributes greatly to the oxygen vacancies concentrations, which favor the oxygen adsorption. Since O_2 tends to react with the reductant prior to NO, an amount of oxygen vacancies can provide an oxygen storage pool to buffer the O_2 effect on the NO reduction over cathodes and thus can improve the selectivity for NO. Meanwhile, the composite with mixed ion-electron conductor (MIEC), in which LSM works as a good electron conductor and GDC as an oxygen-ion conductor, can enhance charge or ion transfer.

4. Results and discussion

4.1. XRD

XRD patterns of the synthesized GDC powders calcined at 1000 °C after 4 h are shown in Fig. 3. A typical cubic fluorite structure for GDC powder can be observed. Main peaks, indexed at about 32.8°, 47.2° and 56.0°, are similar to the fluorite CeO_2 (JCPDS 34-0394), except for the left-shift.

4.2. Electrochemical reduction of NO in the absence of O_2

Fig. 4 presents NO conversion in SSCR based on four LSM-GDC cathodes (LSM-GDC31, LSM-GDC22, LSM-GDC13 and LSM) at 550 and 550 °C when a fixed concentration of NO (2000 ppm)

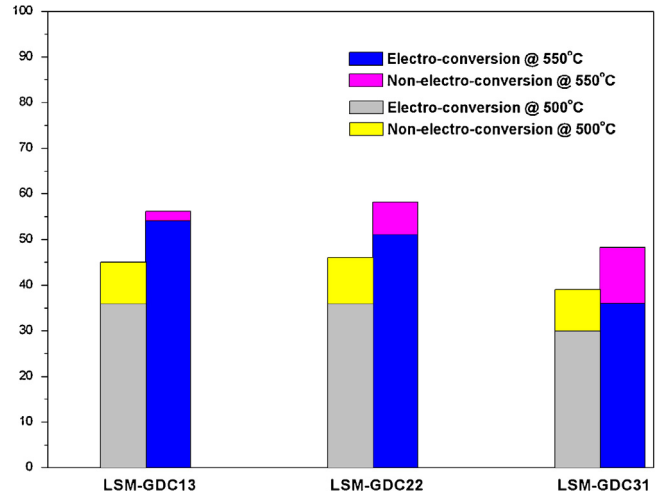

Fig. 5. Electro-conversion and non-electro-conversion of NO in SSCR composed of three cathodes at 500 °C and 550 °C, respectively.

was fed. NO conversion results were collected after reacting for 30 min under two conditions: one is under the open circuit voltage (OCV) condition; the other is under a fixed-voltage. Under both conditions, a slightly higher conversion at 550 °C than that at 500 °C was observed, implying that a higher temperature favors the electrochemical reduction of NO. Under the open circuit condition, NO apparent conversions range from 25% to 30%, independent of the variety of cathodes either at 500 °C or 550 °C. However, when a fixed voltage (0.3 V) was applied under closed circuit condition, NO apparent conversion almost doubles and meanwhile different increase can be found for various cathodes. Under the closed circuit condition at 550 °C, NO apparent conversion is about 35% for the ceria-free LSM electrode, 56% for LSM–GDC13 electrode, 58% for LSM-GDC22 electrode and 48% for LSM-GDC31 electrode. The NO apparent conversion for four samples follows the order: LSM-GDC13 ≈ LSM-GDC22 > LSM-GDC31 > LSM. It is noted that NO apparent conversions can be improved as the GDC amount increases, and a higher NO apparent conversion is achieved for composite cathodes than that for ceria-free cathode. An excessive amount of GDC (for example, LSM-GDC13) contributes little to NO apparent conversion.

Shown in Table 1 are the values of current densities at a fixed-voltage of 0.3 V as well as at OCV when 2000 ppm NO was fed into the cathodes. According to the SOFC principle, the voltage drops with increased currents under closed circuit conditions, just as indicated in Fig. 1S when pure O_2 is fed. Meanwhile the currents become smaller so that they cannot be accurately measured above 0.3 V. Therefore, current data were collected only at the fixed voltage of 0.3 V, instead of as function of different voltages. The results indicate that OCV values do not fluctuate with various amounts of GDC in cathodes, but a slightly higher OCV is found for ceria-free LSM cathode. This result conforms to the case of O_2 absence discussed in hypothesis section. In NO atmosphere, a relative higher OCV obtained is due to ceria-free LSM cathode, which has weak adsorption capability of O_2. Klingenberg et al. also proved by means of DRIFTS that oxygen desorption took place more easily over La_2O_3 and thus the growth of diverse nitrates can be observed [18]. As the only oxygen donor, oxygen from NO decomposition determines OCV. Nevertheless, due to lower pO_2 from the NO direct decomposition, the OCV for LSM cathode in NO atmosphere is still much lower than that in the flowing air (OCV = 1.01 V).

On the other hand, an extreme low current close to zero is obtained at the fixed voltage of 0.3 V for the ceria-free LSM cathode, whereas current density ranging from 10 to 20 mA cm^{-2} can be

achieved for cathodes containing GDC. It indicates that the electrochemical reactions can be promoted under closed circuit conditions for LSM-GDC cathodes. The highest current is achieved with LSM-GDC13, while the lowest current obtained with LSM-GDC31. The results coincide with the enhancement of NO conversion under closed circuit conditions shown in Fig. 4. The difficulty in transferring mobile oxygen from LSM to electrolyte probably is responsible for the extreme low current detected over ceria-free LSM cathode, which also can be further interpreted in the following EIS analysis. The current passing through the whole circuit at 0.3 V greatly promotes the NO conversion over the cathodes, which has been ascribed to the electrochemical promotion of catalysis (EPOC) as suggested Huang and Ni et al. [19,20]. According to the current values and the Faraday Law, NO apparent conversions can be separated into NO electro-conversion and NO non-electro-conversion in Fig. 5. At 550 °C, NO electro-conversions for three cathodes vary from 44% to 53%, dominating the apparent conversion. However, the enhancement effects are distinct with the composition variation of cathodes. The increasing GDC contents improve NO electro-conversion as well as current, which will be explained later.

4.3. Electrochemical reduction of NO in the presence of O_2

Fig. 6 gives that NO conversion and current produced at 500 °C over ceria-containing and ceria-free cathodes, respectively, where O_2 contents ranging from 0% to 15% were introduced into 2000 ppm NO. Generally, the introduction of O_2 promotes NO conversion and thus leads to the larger current density (equal to current divided by electrode area), although it is difficult to identify which of NO and O_2 makes more contribution to the current. A synergistic effect that NO conversion is affected by the current density can be observed when the NO + O_2 were fed into the cathodes, similar to that reported by Huang et al. [21]. More specifically, it seems that NO conversion for ceria-free cathode decreases a little with increasing O_2 concentration as shown in Fig. 6(d). However, the cases of ceria-containing cathodes are complicated. In the case of LSM-GDC13 in Fig. 6(a), NO conversion decreases first and then increases when O_2 exceeds 5%. In the other cases in Fig. 6(b) and (c), NO conversion increases with the higher concentration O_2, and especially the increments become influential when the O_2 concentrations range from 5% to 15%. The maximum NO conversion of 85.0% is achieved over LSM-GDC22 cathode when 15% O_2 is introduced, slightly higher than that of LSM-GDC31 (80.3%). Compared to the previous results (NO conversion of ~97% over LSM-GDC or $LSCoFeO_3$-GDC modified by Cu) obtained by Huang et al., the results in this study are still acceptable considering the lower operating temperature and higher inlet NO concentration [8,22]. The presence of O_2 and the current passing through the closed circuit contribute to the higher NO conversion for cathodes containing ceria, compared to ceria-free cathode.

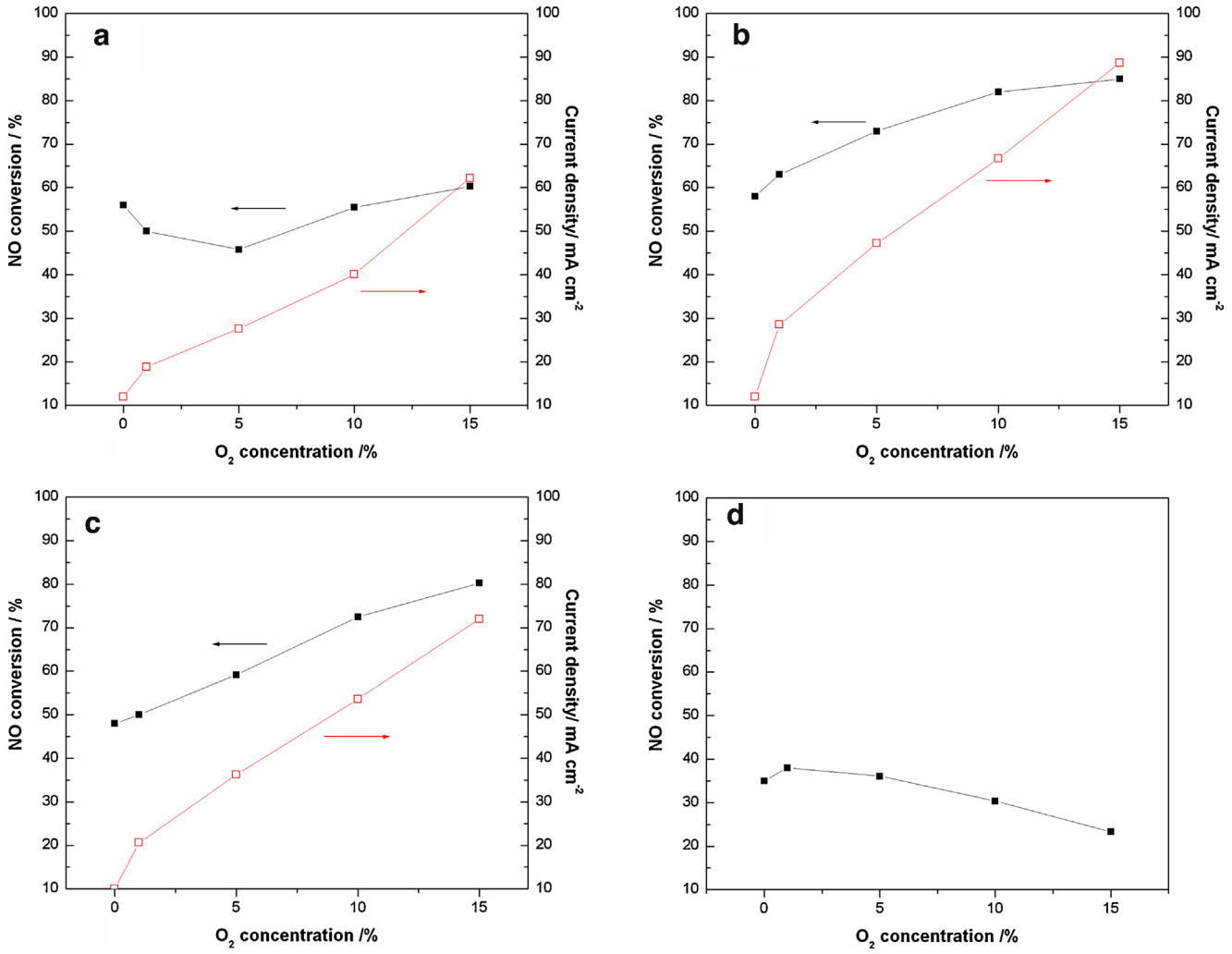

Fig. 6. NO conversion and current density for various cathodes at 500 °C. (a) LSM-GDC13; (b)LSM-GDC22;(c) LSM-GDC31; (d) LSM.

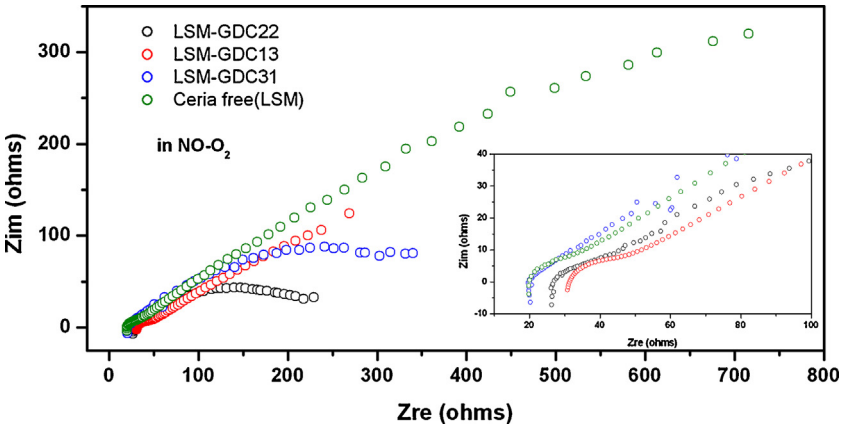

Fig. 7. EIS of symmetric cells composed of LSM-GDC cathodes in the 2000 ppm NO-10%O_2 at 500 °C.

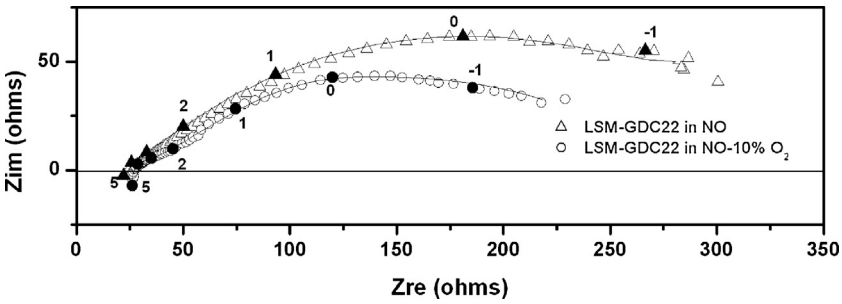

Fig. 8. EIS of symmetric cells composed of LSM-GDC22 cathodes at 500 °C in two atmospheres: 2000 ppm NO and 2000 ppm NO-10%O_2.

Table 1
OCV and current density achieved at 0.3 V in SSCR based on different cathodes exposure to NO.

Temperature/ °C	500		550	
	OCV/V	Current density @ 0.3 V/mA cm^{-2}*	OCV/V	Current density @ 0.3 V/mA cm^{-2}*
LSM-GDC13	0.51	12	0.48	18
LSM-GDC22	0.50	12	0.49	17
LSM-GDC31	0.51	10	0.50	12
Ceria-free	0.62	–	0.67	–

Cell area: 1.77 cm^2.

4.4. Electrochemical reduction of NO over cathodes

EIS measurements for symmetrical cells composed of various cathodes were conducted in three atmospheres, 2000 ppm NO, 10% O_2 and 10% O_2-2000 ppm NO, all balanced by He gas. Nyquist plots for the four symmetrical electrodes in atmosphere of NO-10%O_2 at 500 °C are given in Fig. 7. Ceria-free LSM cathode has the largest arc size and LSM-GDC22 cathode has the smallest arc size, which is the indication of the highest polarization resistance (R_p) for ceria-free LSM cathode and the lowest polarization resistance (R_p) for LSM-GDC22, respectively. The R_p values are in the order of LSM-GDC22 < LSM-GDC31 < LSM-GDC13 < LSM. However, the inset of Fig. 7 shows that the ohmic resistances (R_s) do not follow the order of R_p above, since the intercepts in the high frequency at the real axis represent ohmic resistances (R_s). The R_s values reduce with the decreasing amount of GDC and thus the lowest R_s value is assigned to ceria-free LSM cathode. The results agree with the property of LSM. As one of the electron-conducting materials, the electronic conductivity of pure LSM reaches 200–485 S cm^{-1}, while its ionic conductivity is extremely low in an oxidizing atmosphere [23]. However, a larger R_p value obtained for LSM, representing the charge transfer process, leads to the difficulty of transferring mobile oxygen from triple phase boundaries (TPB, electrolyte/electrode/gas) to electrolyte, even with the assistance of O_2. Therefore, a weak current is undoubtedly observed for the ceria-free LSM cathode as listed in Table 1. Additionally, the effect of overloading GDC amount on the R_p can be interpreted due to the composite microstructure of LSM-GDC proposed by Murray et al. [24]. An optimized amount of ion-conducting material added in the composite cathode can maintain both high TPB densities and high porosities. Consequently, the composite cathodes decrease polarization resistance R_p and improve electrode performance for O_2 reduction [25]. The similar properties can also be observed in the atmosphere of NO-10% O_2 in this study.

The contribution of various physico-chemical processes to the total R_p can be further evaluated by fitting the Nyquist plots, with the help of applying the equivalent circuit $LR_S(RQ)_H(RQ)_M(RQ)_L$. Typically, the electrochemical behaviors for the cathode with the optimized GDC amount (LSM-GDC22) were measured in NO and NO-10%O_2 at 500 °C respectively. Fig. 8 shows that their Nyquist plots as well as their fitting curves. Both in NO-10% O_2 and NO atmospheres, the values of R_s are about 24 Ω cm^2 for LSM-GDC22, which are ascribed to the ion transport in electrolyte. Nevertheless, the polarization resistances in high ($\geq 10^2$ Hz, R_{HF}), medium (10°–10^2 Hz, R_{MF}) and low frequencies ($\leq 10^\circ$ Hz, R_{LF}) vary greatly for the same cathodes in different atmospheres. In NO-10%O_2, R_H,

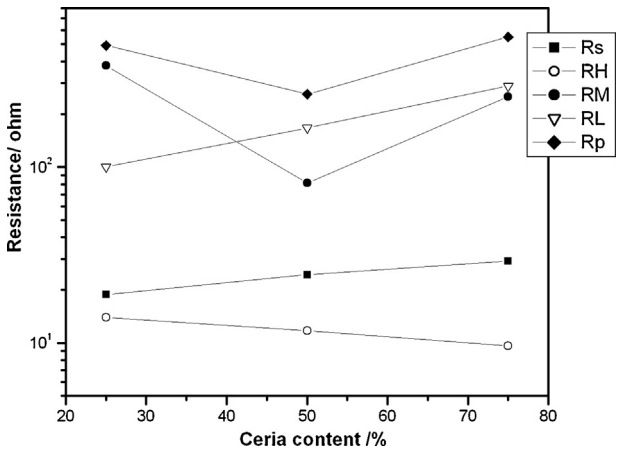

Fig. 9. Series resistances R_s and polarization resistances R_p (including R_p in high, medium and low frequencies) for LSM-GDC at 500 °C in NO-10%O_2.

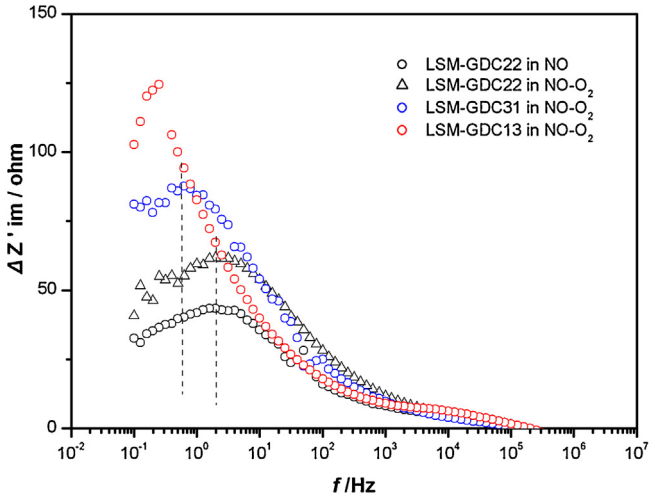

Fig. 10. DIS plots for the LSM-GDC composite cathodes.

R_M and R_L are equal to 11.76, 81.21 and 166.90 Ω cm^2; meanwhile, the corresponding resistances in respective frequency are 10.82, 159.90 and 248.21 Ω cm^2 in NO. The atmospheres in which cathodes work have a distinct effect on the polarization resistance R_p. According to the identification of arcs [26,27], there are at least three arcs in Nyquist plots. Arcs in HF correspond to the charge transfer process, which depends on cathode category. Arcs in MF are attributed to the dissociation of oxygen molecules and the adsorption of oxygen atoms into the cathode, strongly dependent on cathode category and atmosphere. Arcs in LF are associated with the diffusion processes and reaction conversion. In this study, R_H values in two atmospheres are close, indicating that R_H is independent of atmosphere. However, both of R_M and R_L decrease greatly when introducing oxygen into the atmosphere, suggesting that LSM-GDC22 is more active in NO-10% O_2 than that in O_2-free atmosphere.

Even in the same atmosphere, such as NO-10% O_2, the contributions of R_H, R_M and R_L to the total polarization resistance R_p are different for the various cathodes as shown in Fig. 9. With increasing contents of GDC, R_H values decrease a few while R_L values increase. An optimized amount of GDC (50 wt.%) is required with regard to R_M, which greatly accounts for the total R_p. The contribution of R_M to the total polarization resistance R_p also can be magnified by means of differential impedance spectra (DIS) method [28]. The DIS plots for the four cathodes are shown in Fig. 10. In NO-10% O_2

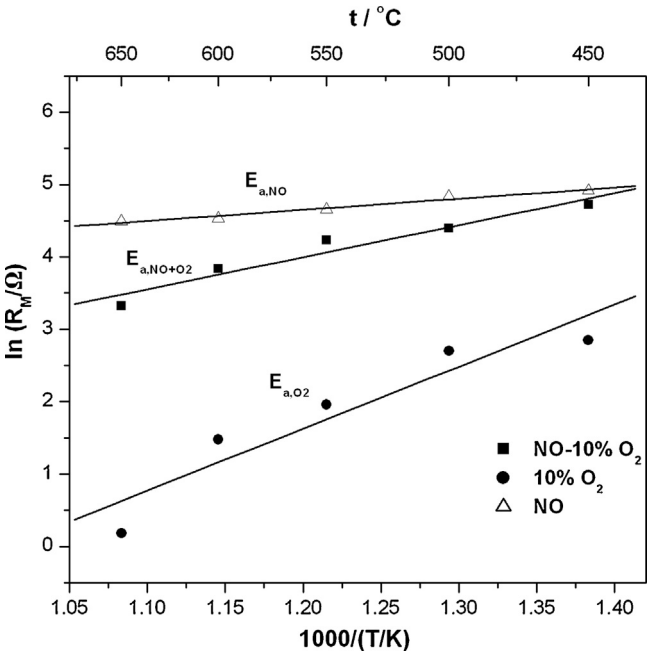

Fig. 11. Arrhenius plots of the R_M for the LSM-GDC22.

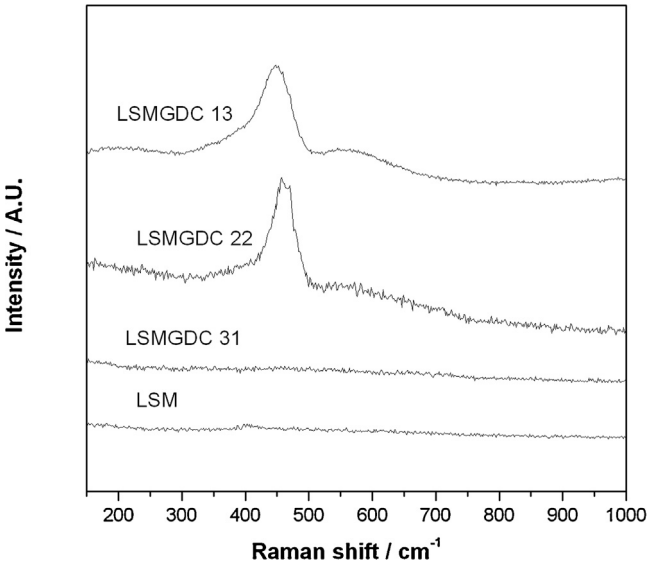

Fig. 12. Raman spectra of LSM-GDC cathodes.

atmosphere, no obvious high-frequency peak appears. The peaks shift from medium frequency to low frequency can be observed in the order of LSM-GDC22, LSM-GDC31 and LSM-GDC13. This indicates that the dissociation and adsorption of oxygen occurring at LSM-GDC22 dominates the cathode reactions, while gas diffusion at LSM-GDC13 dominates the cathode reactions due to the lower porosity. In NO atmosphere, a slight shift to low-frequency takes place for LSM-GDC22 in NO as compared to LSM-GDC22 in NO-10% O_2. In summary, R_M, associate with the dissociation and adsorption of oxygen, dominantly accounts for the total impedance in the mixture of NO and O_2, while R_L, associate with gas diffusion, dominantly contributes to the total impedance in NO atmosphere. The introduction of O_2 makes more difficult for NO decomposition. This result is consistent with the conclusion by Tatsuji, who found that oxygen has an inhibitory effect in the NO decomposition based on manganese oxides [29,30].

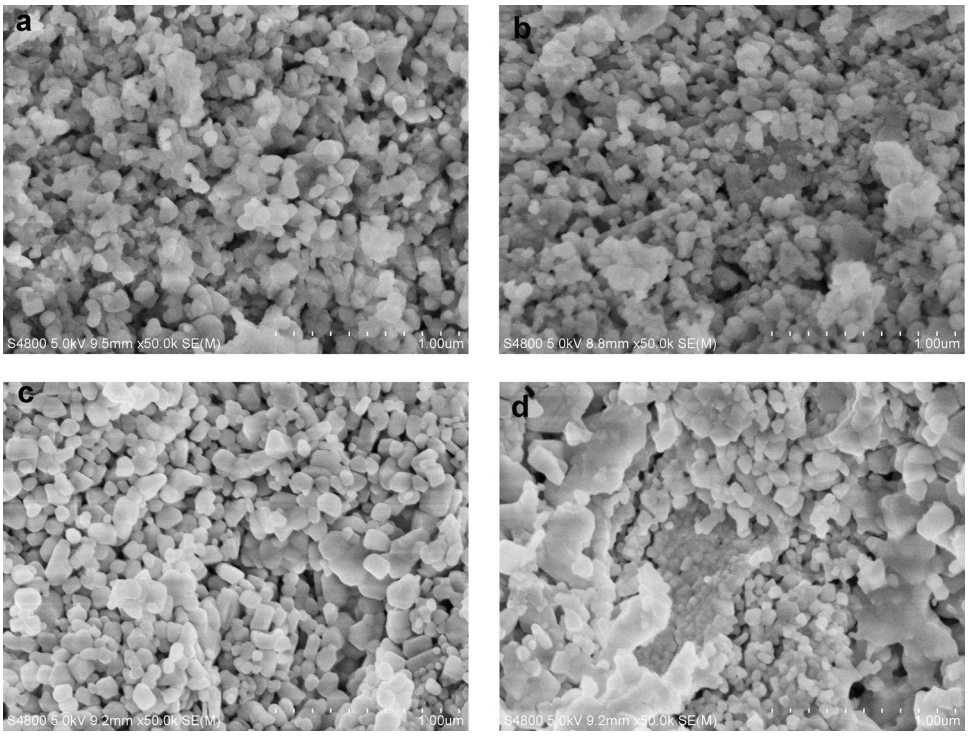

Fig. 13. SEM images of the three LSM-GDC cathodes and LSM ceria-free cathode. (a) LSM; (b)LSM-GDC31;(c) LSM-GDC22; (d) LSM-GDC13.

Since R_M is regarded as the indication of cathode activity towards electrochemical reduction of NO in different atmospheres, the dependence of R_M on temperature is plotted in form of Arrhenius for the LSM-GDC22 in Fig. 11. With elevated temperature, R_M values decrease in all atmospheres. The activation energy E_a of medium-frequency arcs in different atmospheres are $E_{a,NO} = 0.13$ eV, $E_{a,NO+O2} = 0.38$ eV and $E_{a,O2} = 0.74$ eV, respectively. The activation energies E_a, have higher values in O_2-containing atmosphere than in NO atmosphere. An activation energy (0.81 ± 0.04 eV) determined by Kammer in 1000 ppm NO-10%O_2 is higher than these in higher NO concentration (2000 ppm) in this study. It suggests that higher NO concentration favors the decrease of activation energy, which is associated with NO_2 formed around cathodes according to previous literature [31,32]. Kammer et al. believed that LSM based perovskite cathodes were electrochemically active for NO_2 instead of NO. Indeed, a lower activation energy can be obtained in NO atmosphere. Once O_2 is introduced into NO atmosphere, an increase in activation energy is observed. However, the increment of activation energies from NO to NO-O_2 is much smaller than that from N O-O_2 to pure O_2. It also indicates that the O_2 introduction has a limited effect on the NO electrochemical reduction over LSM-GDC22. Additionally, a lower $E_{a,O2}$ value of LSM-GDC than that of LSM-YSZ in Ref. [33] suggests GDC-containing cathodes have better activity for oxygen reduction reactions than YSZ-containing cathode.

4.5. The role of ceria in NO electrochemical reduction

The contributions of R_H, R_M and R_L to the impedances of cathodes with different GDC loadings are also consistent with the electrochemical properties and NO conversions as shown in Fig. 6. In the case of LSM-GDC22 in different atmospheres as shown in Fig. 6(b), the current density becomes larger with the increased O_2 content. The current density is about 10 mA cm^{-2} in O_2-free atmosphere, while the current density rises up to 66.7 mA cm^{-2} in NO-10% O_2 and even to 90 mA cm^{-2} in NO-15% O_2. Meanwhile, NO containing O_2 favors the conversion, and consequently it causes to the reduction of R_L. It can be associated with the formation of intermediate NO_2.

In the cases of various cathodes, the current densities for three cathodes (LSM-GDC13, LSM-GDC 22, LSM-GDC 31) achieved in NO-10% O_2 at 500 °C are 40.1, 66.7, 53.6 mA cm^{-2}, respectively. As discussed above, more GDC doped into the composite cathode (below 50% GDC loading) lead to the decrease in the R_H but increase in R_L. The effect of different GDC loading on the electrochemical performances is associated with the oxygen vacancies. Fig. 12 shows the varieties of oxygen vacancy concentrations with GDC contents, which are determined by Raman spectra. The stokes vibrational F2 g mode observed at 464 cm $^{-1}$ corresponds to cubic fluorite structure of CeO_2. Peaks observed at 550 cm^{-1} and 600 cm^{-1} correspond to intrinsic and extrinsic oxygen vacancies respectively [34,35]. Since the area ratio of the peaks at 550 cm^{-1} and 464 cm^{-1}(A550/A464) represents the oxygen vacancy concentrations, it confirms that the oxygen vacancy concentrations increase with GDC loading. Because O_2 tends to react with the reductant prior to NO, when GDC-containing cathodes are adopted, the oxygen vacancies in cathode with the high contents of GDC can buffer the O_2 effect on the NO electrochemical reduction. Thus the selectivity for NO is enhanced. However, it does not mean that more GDC doped into the cathode is preference, due to the high electron conductivity of LSM as discussed above and the good MIEC composites structure. Fig. 13 presents the microstructure of different cathodes. With increasing GDC loading, uniform microstructures also can be observed. However, an overloading GDC leads to the low porosity and the particle aggregation as shown in Fig. 13(d), which agrees with the higher R_L values obtained in EIS. Generally, LSM particles are surrounded by GDC particles. The feature of good contact between ion conductor and electron conductor within composite cathode, facilitates oxygen derived from the dissociation of O_2 or NO transferring into the TPB, and thus leads to the lower R_H.

Therefore, the composite cathodes containing GDC with MIEC structure have at least two advantages. (1) The oxygen trapped

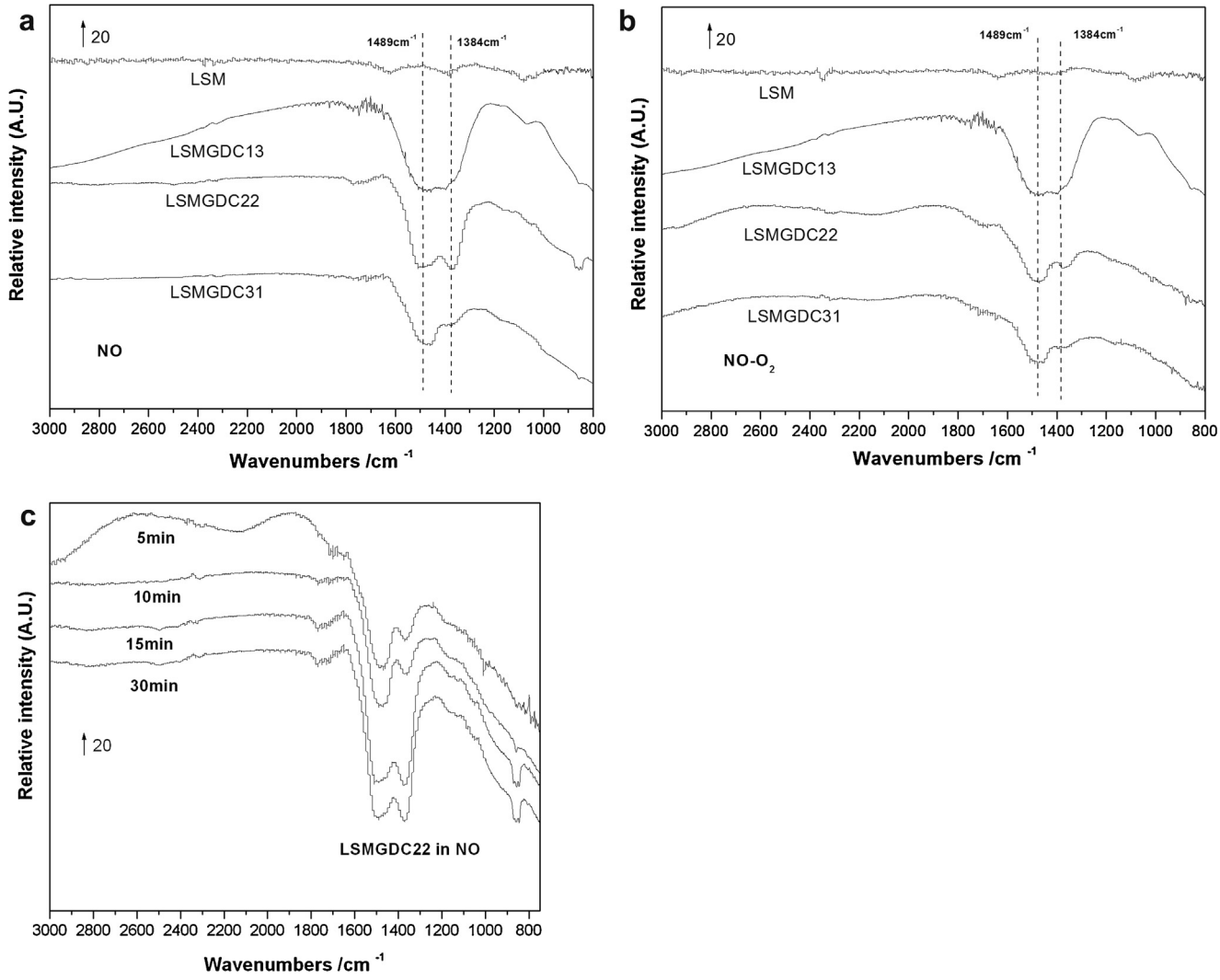

Fig. 14. In situ DRIFT spectra over LSM-GDC cathodes in a flow of 2000 ppm NO (a) and 2000 ppm NO-10%O_2 (b); in situ DRIFT spectra at different time over LSM-GDC22 in a flow of 2000 ppm NO (c).

by oxygen vacancies prefers to take part in the electrochemical reactions, rather than to compete for the active site with NO; (2) A pathway to reduce interfacial resistance by extending the TPB length can be realized in the composite microstructure, similar to the traditional role of MIEC [36].

Fig. 14 shows the DRIFT spectra of three cathodes species at 400 °C in the presence of 2000 ppm NO and 2000 ppmNO-10%O_2 streams, respectively. IR spectra of different cathode materials vary with different GDC amounts, especially at the bands between 1300 and 1800 cm^{-1}. The peak at ~1384 cm^{-1} is assigned to the unidentate NO_3^-, while peak at 1489 cm^{-1} is assigned to unidentate NO_2^- [37]. The assignment of shoulder peaks at 1765 cm^{-1} is consistent with the free gaseous NO_2 molecular. Oppositely, no strong peaks representing nitrite or nitrate species were observed for LSM in NO with or without O_2. It exactly indicates that LSM has weak adsorption for NO, even if the presence of O_2. The oxygen-storage properties of ceria greatly contribute to the creation of nitrite or nitrate species, when LSM-GDC composite cathodes were adopted. Overall, nitrite or nitrate species detected in two atmospheres are associated with the NO adsorption and the reaction with basic anions (e.g. oxygen anion). At high temperature as 400 °C, other nitrite/nitro species are not observed. In the absence of O_2, oxygen derived from NO decomposition may contribute to the formation of these nitrate species. In the presence of O_2, nitrate species detected present weaker peaks than those in the absence of O_2, and the peak intensities degrade with decreasing GDC amount. For LSM-GDC22, peak intensities become large as a function of time in NO atmosphere. It implies that the increasing GDC amount basically maintains the NO adsorption and the reaction over the cathodes, even in excess of O_2.

5. Conclusions

LSM-GDC cathodes with different GDC contents were applied in the solid state cell reactor (SSCR) to realize the electrochemical reduction of NO. By comparison of NO conversion and current produced, the composite cathodes containing GDC are found to possess both good selectivity and relatively high activity in oxygen-rich atmosphere. NO conversion and current density are as high as 80% and 66.7 mA cm^{-2} at 500 °C with the LSM-GDC22, even in excess of oxygen (10% O_2). However, overloading GDC leads to a low porosity and particle aggregation. EIS, Raman and DRIFT spectra prove that Gd-doped ceria plays an important role in the improvement of selectivity and activity towards NO electrochemical reduction.

Acknowledgments

This work was supported by the National Natural Science Funds of China (Grant No. 21207064 and No.51302135) and 333 Talents Project of Jiangsu Province (BRA2013225), and Scientific Research Project of Environmental Protection Department of Jiangsu Province (2015015).

Appendix A. Supplementary data

Supplementary data associated with this article can be found, in the online version, at http://dx.doi.org/10.1016/j.apcatb.2016.02.029.

References

[1] T.D. Elmøe, R.Z. Sørensen, U. Quaade, C.H. Christensen, J.K. Nørskov, T. Johannessen, Chem. Eng. Sci. 61 (2006) 2618–2625.
[2] S. Roy, M.S. Hegde, G. Madras, Appl. Energy 86 (2009) 2283–2297.
[3] T. Kobayashi, S. Morishita, K. Abe, H. Iwahara, Solid State Ionics 86–88 (Part 1) (1996) 603–607.
[4] T. Hibino, K. Ushiki, Y. Kuwahara, Solid State Ionics 98 (1997) 185–190.
[5] K.K. Hansen, Appl. Catal. B 100 (2010) 427–432.
[6] K.K. Hansen, E.M. Skou, H. Christensen, T. Turek, J. Catal. 199 (2001) 132–140.
[7] T.J. Huang, S.H. Hsu, C.Y. Wu, Environ. Sci. Technol. 46 (2012) 2324–2329.
[8] T.J. Huang, C.H. Wang, J. Electrochem. Soc. 158 (2011) B1515–B1522.
[9] T.J. Huang, C.Y. Wu, C.C. Wu, Chem. Eng. J. 168 (2011) 672–677.
[10] K. Hamamoto, Y. Fujishiro, M. Awano, J. Electrochem. Soc. 155 (2008) E109–E111.
[11] K.K. Hansen, Mater. Res. Bull. 48 (2013) 3274–3277.
[12] M. Adamowska, A. Krztoń, M. Najbar, J. Camra, G. Djéga-Mariadassou, P. Da Costa, Appl. Catal. B 90 (2009) 535–544.
[13] A.M. Hernández-Giménez, D. Lozano-Castelló, A. Bueno-López, Appl. Catal. 148–149 (2014) 406–414.
[14] L.A. Chick, L.R. Pederson, G.D. Maupin, J.L. Bates, L.E. Thomas, G.J. Exarhos, Mater. Lett. 10 (1990) 6–12.
[15] J. Nielsen, J. Hjelm, Electrochim. Acta 115 (2014) 31–45.
[16] A. Leonide, B. Rüger, A. Weber, W. Meulenberg, E. Ivers-Tiffée, J. Electrochem. Soc. 157 (2010) B234–B239.
[17] D. Chen, R. Ran, K. Zhang, J. Wang, Z. Shao, J. Power Sources 188 (2009) 96–105.
[18] B. Klingenberg, M.A. Vannice, Appl. Catal. B 21 (1999) 19–33.
[19] T.J. Huang, C.Y. Wu, Chem. Eng. J. 178 (2011) 225–231.
[20] X. Wang, Y. Shi, M. Ni, N. Cai, Chem. Eng. J. 280 (2015) 1–8.
[21] T.J. Huang, C.L. Chou, Electrochem. Commun. 11 (2009) 477–480.
[22] T.J. Huang, C.L. Chou, J. Electrochem. Soc. 157 (2010) P28–P34.
[23] S. Jiang, J. Mater. Sci. 43 (2008) 6799–6833.
[24] E. Perry Murray, S.A. Barnett, Solid State Ionics. 143 (2001) 265–273.
[25] S. Lee, N. Miller, M. Staruch, K. Gerdes, M. Jain, A. Manivannan, Electrochim. Acta 56 (2011) 9904–9909.
[26] J. Shao, K.K. Hansen, J. Electrochem. Soc. 160 (2013) H494–H501.
[27] R. Barfod, M. Mogensen, T. Klemenso, A. Hagen, Y.-L. Liu, P.V. Hendriksen, J. Electrochem. Soc. 154 (2007) B371–B378.
[28] S.H. Jensen, A. Hauch, P.V. Hendriksen, M. Mogensen, N. Bonanos, T. Jacobsen, J. Electrochem. Soc. 154 (2007) B1325–B1330.
[29] T. Yamashita, A. Vannice, J. Catal. 163 (1996) 158–168.
[30] L. Brewer, E. Brackett, Chem. Rev. 61 (1961) 425–432.
[31] R.M.L. Werchmeister, K.K. Hansen, M. Mogensen, J. Electrochem. Soc. 157 (2010) P107–P112.
[32] R.M.L. Werchmeister, K.K. Hansen, M. Mogensen, J. Electrochem. Soc. 157 (2010) P35–P42.
[33] M.J. Jørgensen, M. Mogensen, J. Electrochem. Soc. 148 (2001) A433–A442.
[34] A. Kumar, S. Babu, A.S. Karakoti, A. Schulte, S. Seal, Langmuir 25 (2009) 10998–11007.
[35] Z.Y. Pu, J.Q. Lu, M.F. Luo, Y.L. Xie, J. Phys. Chem. C 111 (2007) 18695–18702.
[36] T. Klemensø, C. Chatzichristodoulou, J. Nielsen, F. Bozza, K. Thydén, R. Kiebach, S. Ramousse, Solid State Ionics 224 (2012) 21–31.
[37] A. Trovarelli, Cat. Rev. 38 (1996) 439–520.